On Merging Image Registration and Focusing: A High-Resolution COTS SAR Application

Juha Jylhä

juha.jylha@patriagroup.com

Minna Väilä

minna.vaila@patriagroup.com

Marja Ruotsalainen

marja.ruotsalainen@patriagroup.com

Juho Uotila
Patria Aviation Oy, Systems – FINLAND

juho.uotila@patriagroup.com

Patria Aviation Oy, Systems & Integrations Operations
FINLAND

ABSTRACT

Synthetic aperture radar (SAR) imaging using a small and lightweight aircraft, such as a drone, sets special requirements on the image formation. Such an aircraft is unable to maintain strictly straight and level flight as it is easily susceptible to the small effects of the atmosphere, such as wind. With conventional SAR methods, a highly fluctuating flight trajectory leads to compromises in image focusing causing distortions in the image. In addition, harsh inaccuracies emerge when registering the image with other information sources: other SAR images of the same scene or geographic information, such as maps or orthoimages. The integration of multiple sources or multiple angles of view improves the detection, recognition, and identification of the objects in the image. In this paper, we consider combining the registration procedure with the SAR image focusing algorithm. We demonstrate our approach through an experiment using a SAR system consisting of a commercial off-the-shelf (COTS) lightweight drone with a COTS sensor payload: a frequency-modulated continuous-wave (FMCW) radar operating at K-band and synchronized with a navigation unit. An accurately focused and georegistered stripmap SAR image with a resolution of 10 centimeters is reconstructed in the case of a trajectory challenging for conventional methods. The implementation and its relevance to different levels of data fusion, especially image or pixel level fusion, is briefly discussed.

1.0 INTRODUCTION

Ground target detection, tracking, recognition, and identification using information provided by distributed airborne sensor systems have important roles in military reconnaissance, surveillance, and target acquisition (RSTA) operations. Various approaches have been proposed for the fusion of the data collected with distributed acquisition. Especially in applications of automatic target recognition (ATR), the performance may be drastically improved by distributed sensing modalities of different types instead of a single modality. One emerging approach to enhancing the cost-effectiveness of RSTA is swarming, where the decentralized processing complements the performance of the individual platforms and offers the flexibility to overcome

mistakes and defects, or even lost platforms—autonomously based on the swarming rules and algorithms [1],[9].

The conventional sensors for RSTA are electro optical (EO) and infrared (IR) cameras, and synthetic aperture radar (SAR). In this paper, we mainly consider a new reconstruction and registration method for SAR images but we also discuss the applications using the EO, IR, and SAR sensors to provide a wider perspective. The fusion of these modalities can be implemented in the decision level (DLF), the feature level (FLF), or the image level (ILF) [5],[6],[7]. A good discussion on the performance gain attainable with the fusion, i.e. the fusion gain, especially at the feature level using EO, IR, and SAR is given in [5]. The fusion at the highest level of abstraction, i.e. the DLF, forms its result by combining the separate fusion outputs of each individual sensor modality, and thus suffers the drawback of assuming appropriate ATR performance for each of them. By contrast, the FLF allows enhanced performance using separately extracted features of supplementary information between the modalities. However, correctly associating the features between the sensor modalities requires some additional processing and introduces a possible error source to the FLF compared to the DLF. The fusion at the lowest level of abstraction, i.e. the ILF, performs the fusion with the image pixels. While being the most complicated technique computationally and algorithmically, it exhibits the highest potential. The multimodal ILF using EO, IR, and SAR images provides new dimensions for the pixels of an individual image and thus ushers in the dawn of next-generation ATR features.

In this paper, we present a new approach to SAR image formation and registration. The primary result of the procedure is a reconstructed SAR image, but SAR image registration to SAR, EO and IR images as well as SAR georegistration are also discussed. The principle depends on the sensor modalities used in the fusion. The following registration modes are considered.

1. Registering a SAR image to another SAR image produces a pixel-level registration between the two SAR images.

2. Registering a SAR image to an EO or IR orthoimage produces a pixel-level registration between the SAR image and the EO or IR orthoimage. Since the orthoimage has been georegistered, the resulting SAR image will have a georegistration, as well.

3. Registering a SAR image to the ground truth produces a registration between the SAR image and a set of the real-world positions, i.e. a georegistration.

The modes 1–2 may include either the FLF or ILF, but the implementation of the ILF is significantly supported by the distortion corrections in the SAR image and its accurate registration. The ground truth information in the third registration mode is external information of the imaged scene, e.g. locations of corner reflectors or other known and located point-like targets in the scene.

We demonstrate the approach using the data produced by a COTS SAR system in a small drone platform, which we introduced in [3]. The K-band FMCW radar produces linear frequency sweeps from 24 to 26 GHz resulting in the range resolution of 7.5 centimeters. Employing antennas with beamwidth of 16° and sweep repetition frequency of 1 kHz, the maximum platform velocity for this system is 11 m/s that is allowed to prevent doppler and cross-range ambiguities. Previously, we have proposed some improvements to SAR image reconstruction and focusing, in e.g. [4],[11],[12]. In this paper, the method we use for image reconstruction follows the basic principles of the back-projection algorithm [4] and is called the matched kernel (MAKE) method [4]. We employ the phase gradient autofocus (PGA) [13],[10] and propose some modifications to it for the distortion corrections and more accurate registration of the result. Our main contribution is to combine the focusing and registration into the same algorithm.

The outline of the paper is as follows. In the next two sections, we describe the method for image reconstruction through the experiment with the COTS SAR system and present the reconstructed stripmap

SAR images. Finally, in section 4.0, we discuss the presented method and achieved results and give the conclusions.

2.0 THE SAR IMAGE FORMATION AND FOCUSING APPROACH

The SAR imaging approach consists of several steps and algorithms. In this paper, we give an overview of the approach via the block diagram shown in Figure 1 and illustrate each of its blocks with an example.

The approach is demonstrated through the data produced by a COTS SAR system operating on the K-band with a bandwidth of 2 GHz. The operation and the available performance of the system is affected by the relatively inexpensive COTS modules, including the FMCW radar, which have their limitations. To diminish their influence, some preprocessing is performed on the measured data: the measured samples are calibrated, erroneous samples are cleaned or removed, and the imaged area is determined. After these operations, we reconstruct a preliminary SAR image using the flight trajectory from the navigation system. These navigation data are inadequate for a high-quality focused image, but we can use this image to detect the dominant scatterers and associate them to the existing information of the scene. Using the knowledge about the registered scatterers, we perform the image focusing and initiate it with the flight trajectory from the navigation system. The focusing procedure corrects the highly fluctuating trajectory in all three dimensions based on the range of the antenna to the scatterers. The range is determined based on the phase gradient from the radar data as a function of time. For the focusing procedure to converge, there need to exist enough distinguishable scatterers in the imaged scene. Due to the accuracy of the trajectory correction, we use the backprojection algorithm to reconstruct the image in the three-dimensional reference frame and no other focusing is necessary. In the block diagram in Figure 1, the point of accepting the result provides a possibility for several iterations of the focusing procedure. In our tests, only one iteration was sufficient. The resulting image is accurately registered to the prior information describing the positions of the dominant scatterers. If the prior information is georegistered, the resulting image pixels will be accurately defined by their three-dimensional positions (e.g. as the true geographic coordinates in the World Geodetic System 84), with only negligible geometric distortions in the image. The same procedure can be employed to reconstruct a SAR image registered to a previous SAR image or to other information sources of the scatterer positions.

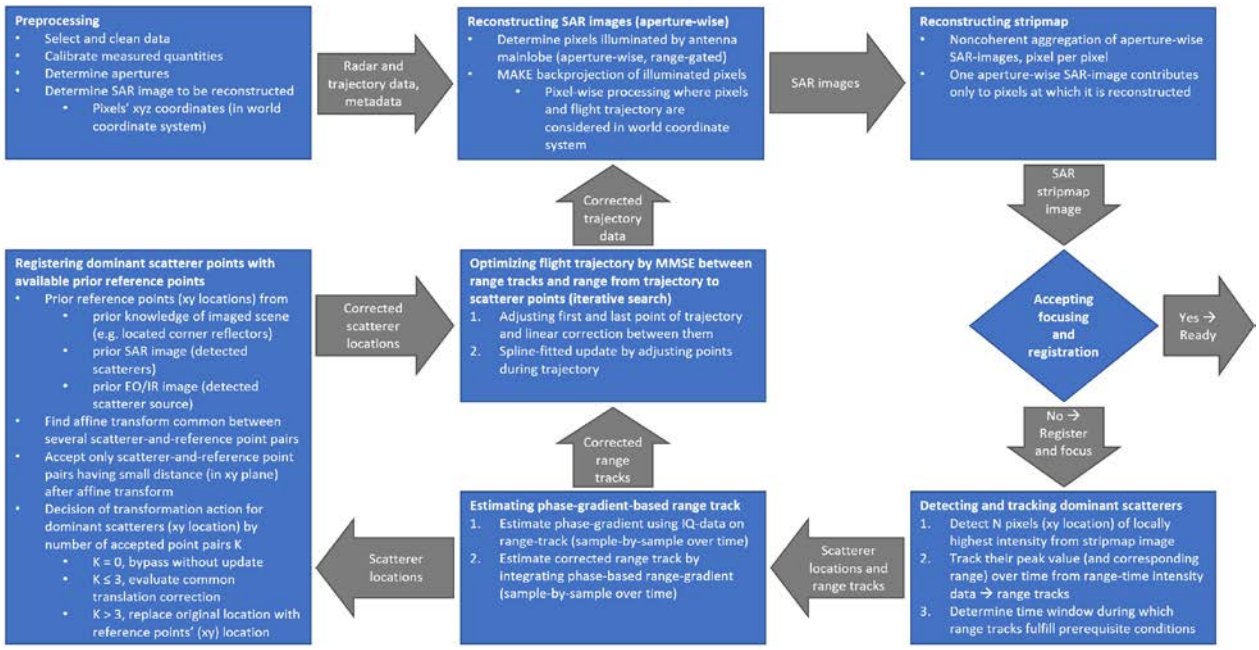

Figure 1: The block diagram for the proposed SAR imaging approach. The PGA and (geo)registration are fused into one algorithm.

2.1 Reconstructing SAR images and a stripmap

After the preprocessing steps, we apply SAR algorithms in the image reconstruction block as can be seen in Figure 1. We perform the reconstruction with the MAKE method [4] due to its adaptability to arbitrary flight of the SAR platform. We adjust the flight trajectory iteratively to produce an accurate and registered result after applying the PGA and the MAKE backprojection. At the beginning without any autofocusing, the reconstructed SAR image looks like the one presented in Figure 2.

The processing performed in the next block, the stripmap reconstruction, is quite straightforward. The SAR images for each aperture formed by the previous block inhabit all the same pixel coordinate setup. Thus, no interpolation is needed with the stripmap formation. The stripmap image is constructed by computing the noncoherent mean absolute value over the aperture-wise images. Obviously, we take into account which pixels have been illuminated during each of the apertures. Figure 3 gives an example result of a preliminary SAR stripmap image.

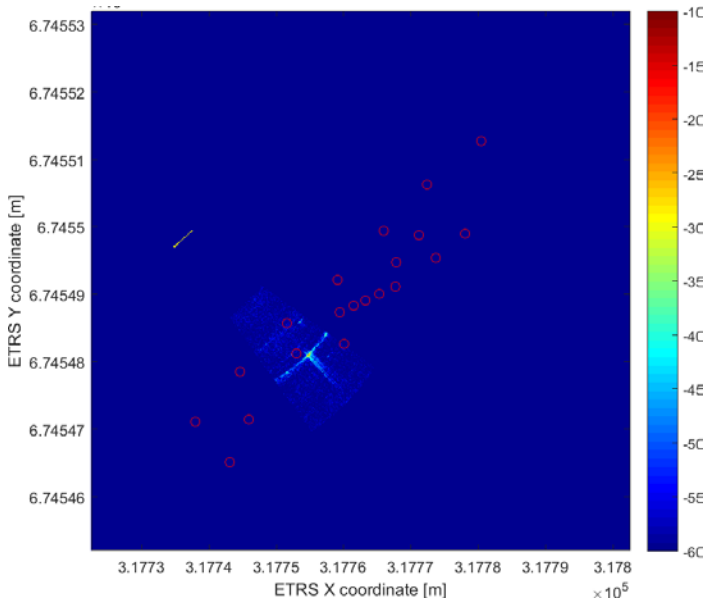

Figure 2: An example of the reconstructed SAR image intensity in the logarithmic color scale. The aperture as well as the matched kernels [7] have been formed based on the flight trajectory provided by the navigation unit of the system (without autofocusing). The yellow line indicates the flight trajectory during the aperture. The response of a large corner reflector is clearly visible in the image, even though no focusing has been performed. The red circles visualize the true locations of the corner reflectors in the imaged scene.

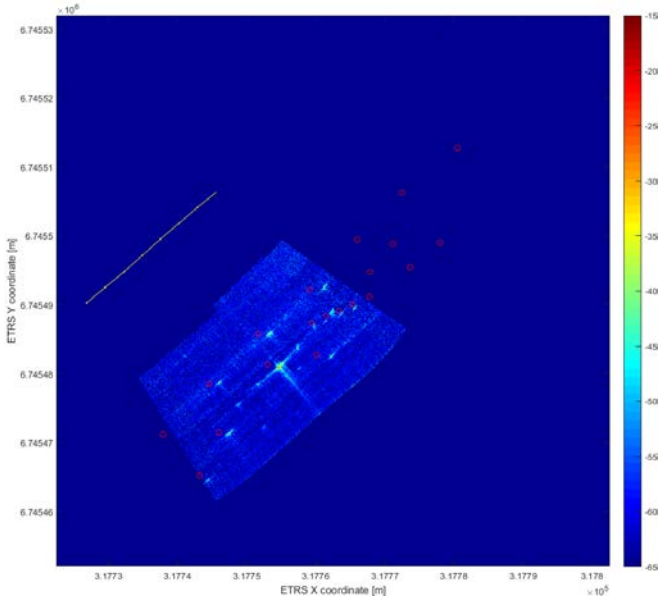

Figure 3: An example of the SAR stripmap image intensity in the logarithmic color scale. The apertures have been formed based on the flight trajectory provided by the navigation unit of the system (without autofocusing). The yellow line indicates the flight trajectory during the stripmap, and the yellow dots mark the start and stop points of the separate apertures. The response of several corner reflectors is clearly visible. The red circles visualize the true locations of the corner reflectors in the imaged scene. Distortions between the preliminary stripmap image and the ground truth are also distinguishable in the image.

2.2 Detecting and tracking the dominant scatterers

We begin the autofocus procedure by detecting and tracking the response of the dominant scatterers in the stripmap image. The stripmap is windowed in time taking the flight-mechanical properties of the SAR platform into account because our aim is a realistic adjustment of the trajectory in the subsequent processing blocks. A good choice for the window length considers the flight-mechanical dependence within the window. The detection of the scatterers, visualized in Figure 4, is based on searching for the intensity peaks and validating them in a similar manner to constant false alarm rate processing by comparing the peak value to the median value in the surrounding pixels. To track the range in the range-time domain, we first calculate the Euclidean distance between the trajectory and the scatterer points, which are both defined in the world coordinate system, as a function of time. Then, we determine the more accurate range at the intensity maximum in the vicinity of the preliminary range track in the range-time domain. At the same time, we ensure that the ridge of the found maxima follows a smooth curve and that the maximum intensity remains higher than a threshold value tied to the intensity in the surrounding range vicinity. Thus, the start and stop time of each track is determined. An example of the result of this process is shown in Figure 5.

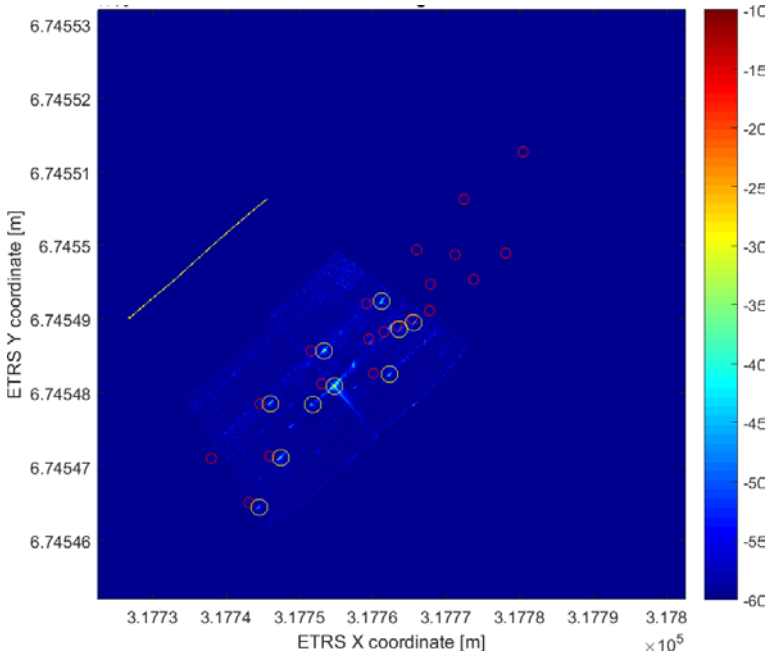

Figure 4: The result of the detection of the locally highest intensity points for the stripmap image shown in Figure 3. The ten detections are highlighted with the yellow circles.

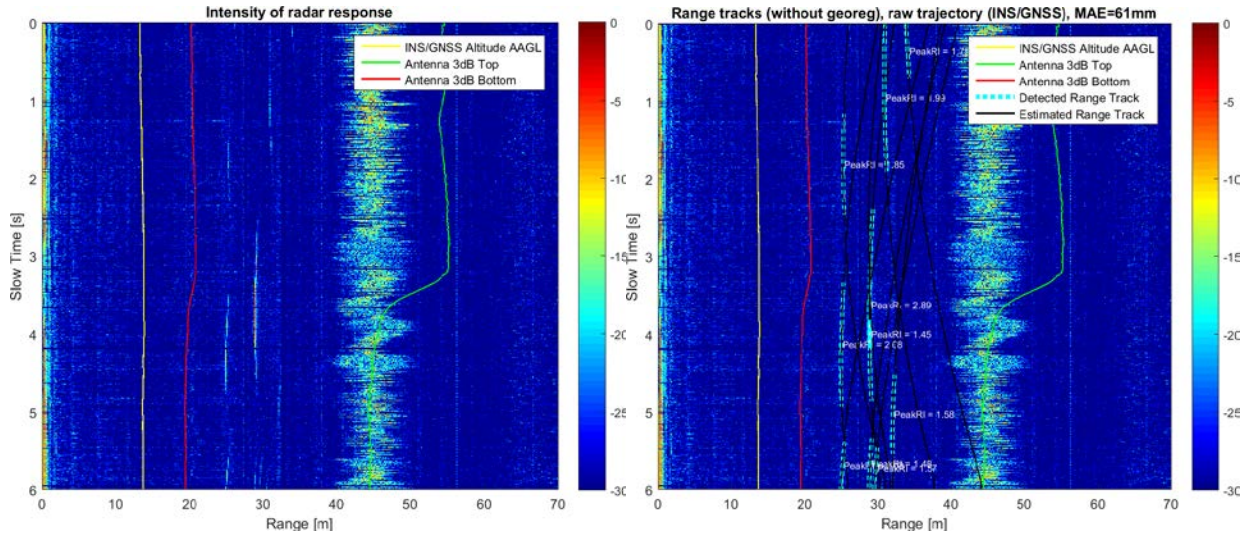

Figure 5: An example of the range tracking. On the left, the logarithmic radar intensity data are visualized in the range-time domain within the selected time window. The window corresponds to the stripmap images in Figures 3 and 4. On the right, the radar intensity data are presented overlaid with the range tracks: the estimates during the whole trajectory are presented with the black curves, and the detections with the cyan curves. The yellow curves are the altitude estimates of the radar platform. The red curves indicate the front edge and the green curves the far edge of the antenna mainlobe, i.e., the illuminated-ground part of the range domain. Many disturbances can be observed in the radar data.

2.3 Estimating phase-gradient-based range tracks

The range tracks resulting from the previous block do not have the accuracy required for the autofocus in the K-band. Thus, we employ a phase-gradient-based range adjustment. Figure 6 gives an example of the range

track, obtained by the phase-gradient, compared with the original intensity-based range track that is acquired from the radar range-time data. If the range adjustment fails due to evident mismatch between the original range track and the phase-gradient-based one, the range track in question is declared as invalid and eliminated from the PGA and registration procedure.

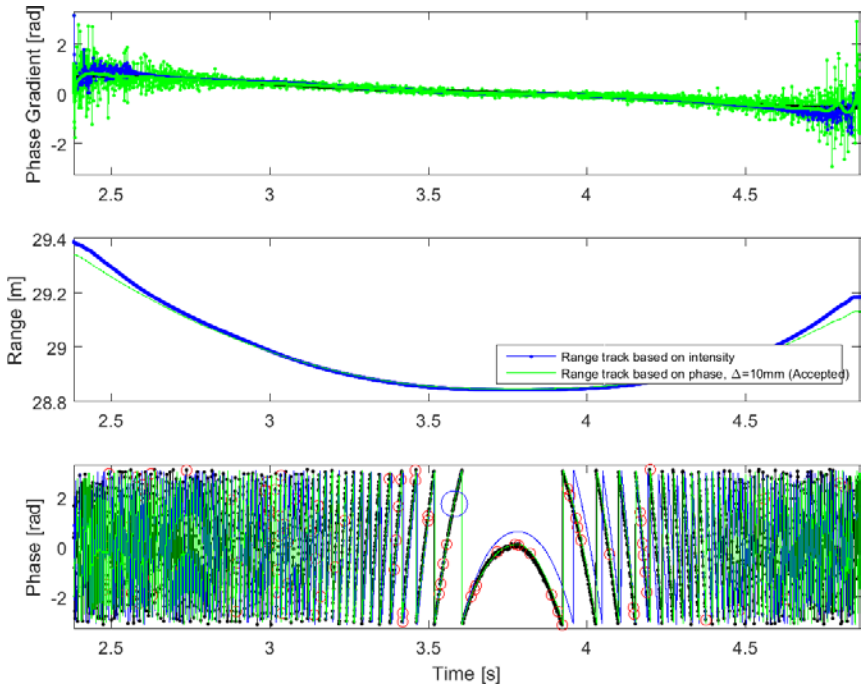

Figure 6: The phase-gradient range tracking result is illustrated with the green curves and the intensity-based range track with the blue curves. In the bottom figure, the black dots indicate valid samples and the red circles invalid samples of the intensity-based range track. The validity of the samples is determined from the radar data in the data cleaning procedure (in the preprocessing block in Figure 1).

2.4 Registering the dominant scatterer points with the available prior reference points

The range track adjustment and validation performed in the previous blocks verified the existence of the dominant scatterers in the SAR image. Next, we determine the more exact locations for the dominant scatterer points in the SAR image. This is performed based on the prior information: the known locations of the potential scatterers. If the association between the detected points and the prior reference points is successful, we can supplement the autofocus with this information improving it drastically. The association between these points is conducted by estimating a common affine transform for them. The affine transform cannot be determined explicitly due to the inherent incompatibility between the point sets, which practically never consist of exactly the same points. In addition, every point has at least a small error in their detected location. The classic principle of the random sample consensus (RANSAC) [2] is followed. The result is illustrated in Figure 7. The translation correction (i.e. the affine transform) that is common to all the valid point pairs can be seen in the result. The replaced scatterer locations as well as the found transformation matrix are returned from this considered block of Figure 1.

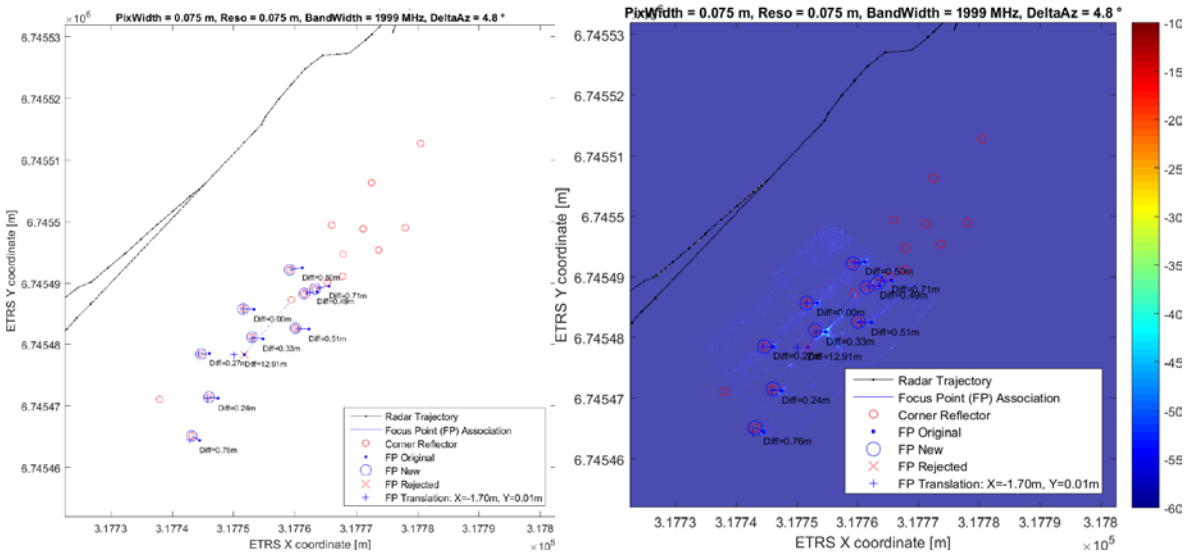

Figure 7: An intermediate result of registering the dominant scatterers with the true locations of the corner reflectors. The locations are illustrated on a blank background on the left and overlaid on the SAR stripmap image on the right. The blue dots mark the original locations of the detected scatterers, i.e., the original focus points. The blue circles indicate their location after the common translation correction that is used for validating the association. The red circles indicate the true locations of the corner reflectors used as the reference in the association algorithm.

2.5 Optimizing the flight trajectory

Our modified PGA iteratively adjusts the flight trajectory of the SAR platform, so that in the next phase we can run the MAKE backprojection using the updated trajectory and obtain a SAR image of higher quality. This trajectory optimization is based on minimizing the mean squared error (MSE) between the range tracks and the range from the trajectory to the scatterer locations. All the range tracks are incorporated into the objective function. This is important because the domain where the trajectory is optimized has multiple degrees of freedom. Flight-mechanical inertia causes dependence between the consecutive trajectory sample points that reduces the problem and thus the number of points that need to be be spatially adjusted. To converge properly, the method requires several phase-gradient-based range tracks, i.e. the validated dominant scatterers, on which the objective function is based. Preferably, those scatterers are located all over the stripmap SAR image. This increases the validity of the spatial adjustments also in the altitude dimension.

First, we perform coarse spatial adjustments by searching a new starting and ending location and translating the whole trajectory between them in a linear manner. This can be aided by the affine transformation matrix found in the previous block. Second, we iteratively fit an N-point spline that replaces the trajectory increasing the N at each iteration. We randomize new spline points on each iteration, similarly to the approach of simulated annealing. The trajectory is accepted only if its MSE is lower than the previous minimum. An example result is illustrated in Figure 8.

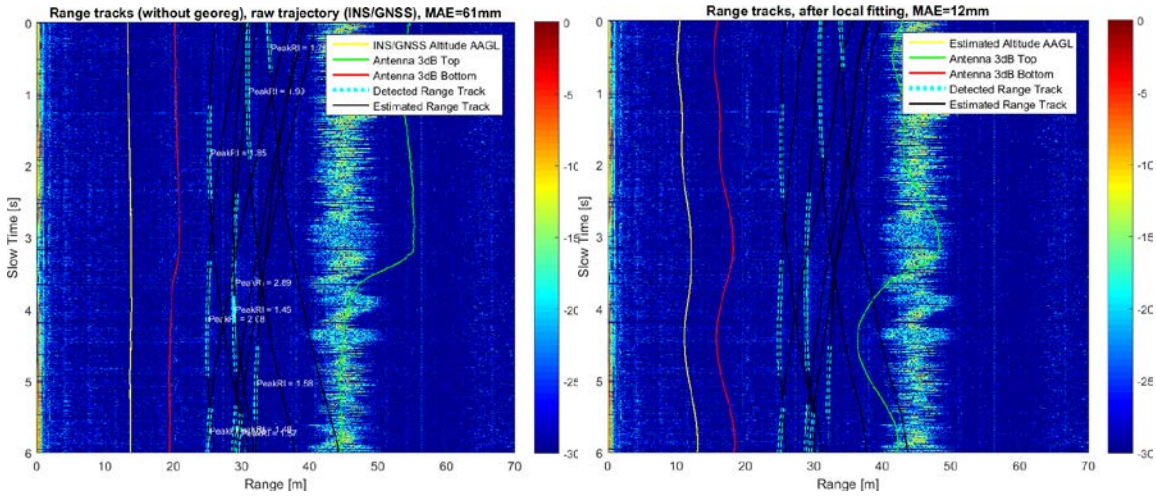

Figure 8: The trajectory optimization illustrated using the range track visualization. The initial situation is shown on the left and it is the same image as presented in Figure 5. The result after the trajectory optimization is shown on the right. The black lines indicate the estimated scatterer tracks during the entire trajectory and the cyan lines the detected response. The yellow lines correspond to the altitude estimate of the radar platform. The red line indicates the front edge and the green line the far edge of the antenna mainlobe, i.e., the illuminated-ground in the range domain.

3.0 RESULTS

We consider the potential of the proposed approach by presenting four stripmap SAR results with different properties in Figure 9. All the presented four images are reconstructed with the methods shown in Figure 1 but using different imaging modes. As can be seen, the MAKE backprojection produces a result that is appropriate for many purposes even without autofocusing. The PGA enhances the image quality as the point spread function is sharper than without autofocusing, which can be judged by the shape of the corner reflector responses in the SAR images. This enhancement is achieved whether or not the PGA is aided by the registration or not. The two bottom images in Figure 9 represent the imaging modes that use the registration procedure. In those two modes, the result reveals the pixel-level match resulting from the registration. The major differences emerge in the area highlighted in the images for which there is two separate stripmap SAR images reconstructed within back and forth flying. In that area, a double response from each corner reflector is seen in the images without the registration, and unified responses emerge in the images with the registration. When comparing the two results with registration, the difference is in the accuracy of matching with the ground truth locations. The georegistered result allows the highest potential for RSTA purposes.

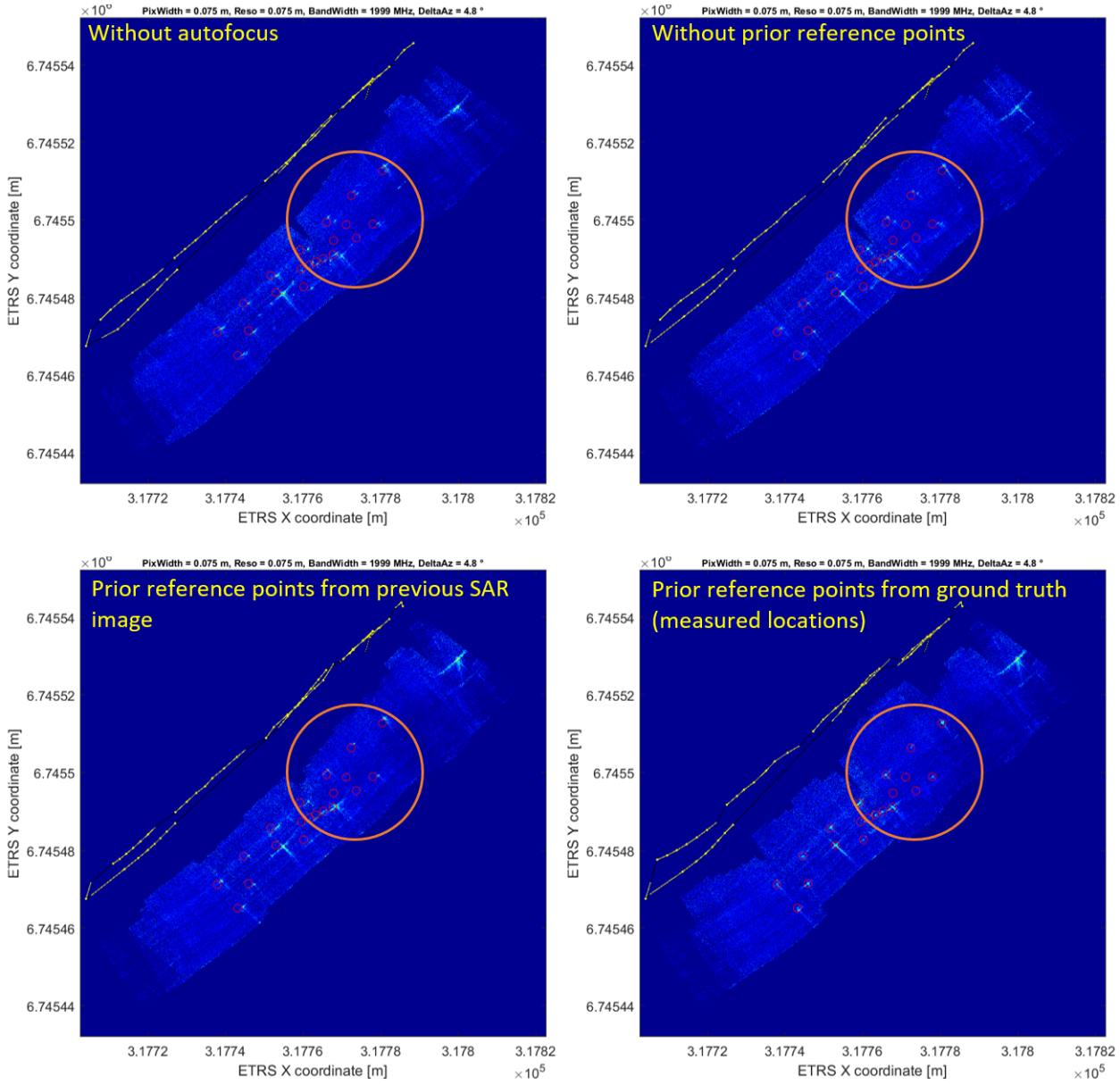

Figure 9: Short-range stripmap SAR images in four different imaging modes. The trajectory of the imaging platform is shown in yellow lines and the yellow dots indicate the starting points of the apertures. The color values of the background represent the logarithmic intensity of the SAR image. The small red circles indicate the true locations of several corner reflectors in the scene. The area highlighted with an orange circle has been imaged two times and the results have been combined by averaging. In that area, the differences in registration are clear when comparing the different imaging modes. The image on the top left has been reconstructed without the autofocus. The image on the top right has been reconstructed using the PGA but without prior information of the reference points, i.e., it is not registered. The image on the bottom left has been registered to another SAR image, i.e., reconstructed supplementing the autofocus (PGA) with the detected scatterers of the previous SAR images (of the same flight). On the bottom right, the georegistered image (the PGA supplemented with the true scatterer locations) has only minor distortions and deviations.

4.0 DISCUSSION AND CONCLUSIONS

In this paper, we presented a novel reconstruction and registration method for SAR images. As was shown in Section 3.0, the method can be applied to the registration of a SAR image with known scatterer locations or to another SAR image.

In this paper, we presented a novel reconstruction and registration method for SAR images. As was shown in section 3.0, the method can be applied to the registration of a SAR image with known scatterer locations or to another SAR image.

In addition, a SAR image can be registered to an EO or an IR image. The SAR, EO, and IR sensors operate on different parts of the electromagnetic spectrum and thus produce orthogonal and complementary information compared with each other. The different sensor modalities exhibit the physical properties of the target very differently. For each sensor type, the quality of the information varies depending on the target properties, the environmental circumstances, the imaging distance, and the possible camouflage of the target. Employing either the DLF or the FLF on the images enhances the probability of detection and reduces the number of incorrect classifications in the recognition and the identification of targets. The benefits of the image fusion are greater than simply selecting the best single sensor result. In addition, the accurate registration between the images enables even greater potential for the FLF and the ILF to be used.

The complementary information of different sensor images can be viewed projected to true geolocations on the ground plane or in a slant view like the EO or the IR image, that in the case of SAR can be called a “pilot-view SAR”. The slant projection enables effective feature or pixel level fusion to the complementary EO and IR images. The method is general enough to suit the registration of various types of images from sensors operating on different parts of the electromagnetic spectrum and not limited to the currently tested SAR, EO, and IR sensors. An example of the SAR image fused with the EO and IR images is shown in Figure 10. The previously introduced COTS system provided these data using the FMCW radar and a commercial FLIR camera with EO and IR sensors. The fusion method used here was a shift invariant discrete wavelet transform (SIDWT) with a Haar wavelet [8]. Prior to the fusion, the SAR image was reconstructed and georegistered using the approach proposed in this paper. Another way to implement the fusion of different image modalities is projecting the slant view images on the ground plane, on which the pixel level fusion can be applied. The proposed SAR reconstruction method allows the georegistration of the SAR image on the ground plane when point-like scatterers with known location exist in the scene.

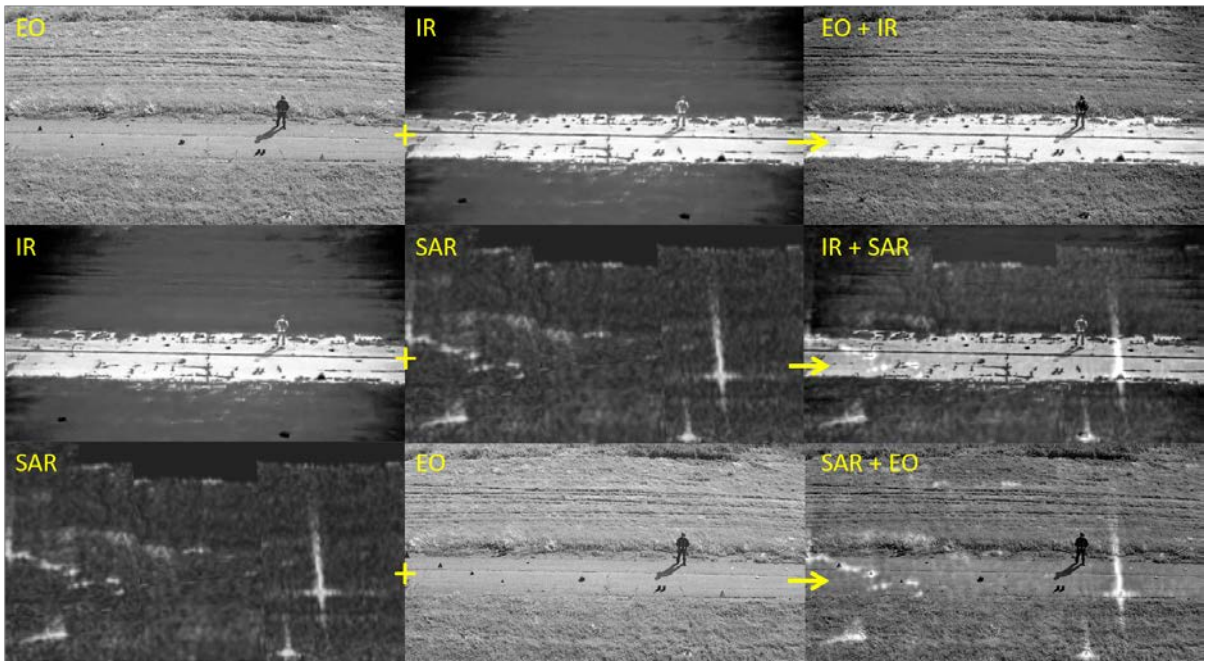

Figure 10: Examples of ILF of SAR, EO, and IR images using SIDWT with a Haar wavelet

The weaknesses of the presented approach concern the computational requirements of the MAKE backprojection and the inherent drawbacks of the PGA. The SAR image reconstruction with the MAKE method allows a challenging flight trajectory (of the imaging platform) during the SAR aperture but involves heavy pixelwise processing. The approach to motion compensation based on the modified PGA implemented in MAKE and iteratively adjusting the flight trajectory provides great benefits but requires several point-like targets to exist in the imaged scene. Without these point-like targets or with only one of them, the method does not converge. Nevertheless, there exist means to reduce the computational burden of the backprojection, and the most typical target scenes are well suitable for the proposed modified PGA. As the backprojection is highly parallelizable, the computational cost can be mitigated with e.g. graphics processing unit (GPU) processing. The prospects of the approach consist of studying various use cases such as testing with different SAR systems and scenes. Several interesting image fusion use cases in FLF and especially in ILF can be anticipated in the field of RSTA.

ACKNOWLEDGMENTS

The authors would like to thank the Finnish Scientific Advisory Board for Defence (MATINE) for funding.

6.0 REFERENCES

[1] Bandala, A.A., Dadios, E.P., Vicerra, R.R.P., and Lim, L.A.G. (2014). Swarming algorithm for unmanned aerial vehicle (UAV) quadrotors – Swarm behavior for aggregation, foraging, formation, and tracking. Journal of Advanced Computational Intelligence and Intelligent Informatics, 18(5), pp. 745-751.

[2] Sauter, J.A., Mathews, R.S., Yinger, A., Robinson, J.S., Moody, J., and Riddle, S. (2008). Distributed pheromone-based swarming control of unmanned air and ground vehicles for RSTA. Proc. SPIE 6962, Unmanned Systems Technology X, 69620C, SPIE Defense & Security Conference, Orlando, FL, USA, Apr 2008.

[3] Kahler, B. and Blasch, E. (2010). Predicted radar/optical feature fusion gains for target identification. Proc. of the IEEE 2010 National Aerospace & Electronics Conference, IEEE, Dayton, OH, USA, Jul 2010.

[4] Kahler, B. and Blasch, E. (2008). Robust multi-look HRR ATR investigation through decision-level fusion evaluation. Proc. of the IEEE 11th International Conference on Information Fusion, Cologne, Germany, Jul 2008.

[5] Kim, J. and Kwag, Y.K. (2014). Multi-sensor fusion based target detection using EO/ SAR. Proc. of the 10th European Conference on Synthetic Aperture Radar (EUSAR), Berlin, Germany, Jul 2014.

[6] Jylhä, J., Tolkkinen, H., Arajärvi, R., Väilä, M., and Ruotsalainen, M. (2019). Synthetic aperture radar imaging using COTS components. XXXV Finnish URSI Convention on Radio Science, Tampere, Finland, Oct. 2019. http://www.ursi.fi/2019/

[7] Jylhä, J., Väilä, M., Perälä, H., Väisänen, V., Visa, A., Vehmas, R., Kylmälä, J., and Salminen, V.-J. (2014). On SAR processing using pixel-wise matched kernels. Proc. of the 2014 11th European Radar Conference (EURAD), Rome, Italy, Oct 2014.

[8] Vehmas, R., Jylhä, J., Väilä, M., Vihonen, J., and Visa, A. (2018). Data-driven motion compensation techniques for noncooperative ISAR imaging. IEEE Transactions on Aerospace and Electronic Systems, 54(1), pp. 295-314.

[9] Vehmas, R., Jylhä, J., Väilä, M., and Visa, A. (2017). Analysis and comparison of multichannel SAR imaging algorithms. Proc. of the 2017 IEEE Radar Conference (RadarConf), Seattle, WA, USA, May 2017.

[10] Wahl, D.E., Eichel, P.H., Ghiglia, D.C., and Jakowatz, C.V. (1994). Phase gradient autofocus – A robust tool for high resolution SAR phase correction. IEEE Transactions on Aerospace and Electronic Systems, 30(3), Jul 1994.

[11] Thompson, D.G., Bates, J.S., and Arnold, D.V. (1999). Extending the phase gradient autofocus algorithm for low-altitude stripmap mode SAR. Proc. of the 1999 IEEE Radar Conference, Waltham, MA, USA, Apr 1999.

[12] Fischler, M.A. and Bolles, R.C. (1981). Random sample consensus: A paradigm for model fitting with applications to image analysis and automated cartography. Communications of the ACM, 24(6), pp. 381-395, Jun.

[13] Lemeshewsky, G.P. (1999). Multispectral multisensor image fusion using wavelet transforms. Proc. SPIE 3716, Visual Information Processing VIII, Orlando, FL, USA, Apr 1999.